ATMOSPHERIC SCIENCE

Asphalt-related emissions are a major missing nontraditional source of secondary organic aerosol precursors

Peeyush Khare[1], Jo Machesky[1,2], Ricardo Soto[1], Megan He[1], Albert A. Presto[3], Drew R. Gentner[1,2,4]*

Asphalt-based materials are abundant and a major nontraditional source of reactive organic compounds in urban areas, but their emissions are essentially absent from inventories. At typical temperature and solar conditions simulating different life cycle stages (i.e., storage, paving, and use), common road and roofing asphalts produced complex mixtures of organic compounds, including hazardous pollutants. Chemically speciated emission factors using high-resolution mass spectrometry reveal considerable oxygen and reduced sulfur content and the predominance of aromatic (~30%) and intermediate/semivolatile organic compounds (~85%), which together produce high overall secondary organic aerosol (SOA) yields. Emissions rose markedly with moderate solar exposure (e.g., 300% for road asphalt) with greater SOA yields and sustained SOA production. On urban scales, annual estimates of asphalt-related SOA precursor emissions exceed those from motor vehicles and substantially increase existing estimates from noncombustion sources. Yet, their emissions and impacts will be concentrated during the hottest, sunniest periods with greater photochemical activity and SOA production.

INTRODUCTION

Recent studies show that nontraditional sources, i.e., volatile chemical products (VCPs) and other non–combustion-related sources, are now dominating emissions of volatile organic compounds (VOCs) in U.S. megacities (*1*, *2*) and are likely major sources of intermediate/semivolatile organic compounds (I/SVOCs), but major knowledge gaps exist (*1*). These VOC and I/SVOC emissions are important precursors to ozone and secondary organic aerosol (SOA), a major component of $PM_{2.5}$ (particulate matter smaller than 2.5 μm in diameter) with substantial public health effects (*3*). They can be classified into three pathways: (i) solvent evaporation, (ii) volatilization of solutes, and (iii) off-gassing of compounds not present in product formulations (e.g., degradation by-products) as is the case with asphalt-related emissions (*1*). Emission time scales from any applied products and materials are highly dependent on temperature, film thickness, and compound volatility and can extend to months or longer for I/SVOCs (*1*). Model results estimate that 70 to 86% of urban SOA in metropolitan Los Angeles comes from the oxidation of primary I/SVOC emissions (*4*). Yet, ambient data show that a substantial (unspecified) fraction of I/SVOCs originate from unidentified, petroleum-related sources other than on-road vehicles (*5*).

Liquid asphalt is a petroleum-based product widely used in cities. With urban areas comprised of 45%+ paved surfaces and 20% roofs (*6*), annual demand is 122.5 million metric tons globally and 27 million metric tons in the United States for the liquid asphalt binder that is then typically mixed with other structural materials (e.g., aggregates) depending on usage (*7*). Its uses include paving (mixed with stone aggregate), roofing, and other consumer, commercial, and industrial products (e.g., sealants). Liquid asphalt binder is a highly viscous complex mixture of nonvolatile petroleum-derived bitumen from crude oil or unconventional deposits. It is vacuum-distilled to an equivalent of 535°C in an effort to remove VOCs, IVOCs, SVOCs, and LVOCs (low-volatility organic compounds) and is typically air-rectified to promote polymerization and stiffness (*8*). While solvents are occasionally used for select applications, it is typically made less viscous by increasing its temperature beyond its softening point. Its chemical composition varies by geologic source, processing methods, and application specifications, with desirable asphalt-bitumen often containing 1 to 7% sulfur (*7*).

Some evidence for asphalt-related emissions during hot application exists from Occupational Safety and Health Administration (OSHA)–focused occupational exposure studies; however, no studies have quantified emission rates or complete source profiles (*9*–*15*). Area source asphalt-related emissions are essentially absent in emission inventories, with the exception of VOC solvent evaporation from cutback asphalt application, a rare (~1%) method compared to hot-mix asphalt that uses no solvents (*1*). Studies of point source asphalt manufacturing facilities have calculated emission factors (EF) for criteria pollutants, greenhouse gases, select polycyclic aromatic hydrocarbons (PAHs), and total organic carbon (*16*–*19*). Occupational exposure–related measurements during hot asphalt application have observed elevated concentrations of VOCs, primary PM, and other hazardous air pollutants and have provided evidence for a broad range of cyclic and acyclic alkanes, single-ring aromatics, and PAHs from hot-mix asphalts (*13*–*15*, *20*–*25*). Yet, industry states that emissions at ambient temperatures are negligible because the manufacturing process removes all potential emissions (*26*). Other past studies on the effects of ambient conditions, especially solar radiation, were limited to asphalt mechanical performance, longevity, and greenhouse gas emissions (*14*, *27*–*34*).

With a large asphalt surface area in the urban built environment and evidence for emissions of reactive precursors, asphalt represents an important potential source of urban SOA precursors (*35*, *36*). Yet, other than emissions of infrequently used solvents during paving, emissions from the asphalt binder itself are poorly constrained and not included in inventories/models due to their understudied emission pathways, long emission time scales, and

[1]Department of Chemical and Environmental Engineering, Yale University, New Haven, CT 06511, USA. [2]Solutions for Energy, Air, Climate and Health (SEARCH), School of Forestry and Environmental Studies, Yale University, New Haven, CT 06511, USA. [3]Department of Mechanical Engineering, Carnegie Mellon University, Pittsburgh, PA 15213, USA. [4]Max Planck Institute for Chemistry, Mainz 55128, Germany. *Corresponding author. Email: drew.gentner@yale.edu

source profiles (i.e., volatility and isotopic signatures) that could confuse them with vehicular emissions in ambient data (*1*). Furthermore, variations in temperature, solar irradiation, and oxidant exposure vary greatly throughout asphalt's life cycle (Fig. 1A). Temperatures range from 80° to 140°C for storage and 120° to 160°C for paving application, and in-use pavement reaches 47° to 67°C in summer (*37*–*41*) [75°C for roofs (*42*, *43*)]. More information on asphalt paving and ambient conditions can be found in sections S1 and S2, respectively.

Our overall objective is to determine asphalt-related gas-phase emissions and potential SOA production under typical environmental conditions during different life cycle stages. Specifically, we (i) subject freshly obtained real-world samples of commonly used performance grade (PG) 64-22 road asphalt to temperature (40° to 200°C) and artificial solar radiation stresses in an experimental chamber; (ii) develop detailed time- and temperature-dependent emission factors and source profiles for the speciated complex mixture of VOCs, IVOCs, SVOCs, and LVOCs; (iii) confirm observations against other common asphalt-containing materials/products and targeted ambient field measurements following asphalt application; and (iv) estimate the magnitude of urban asphalt-related emissions and potential SOA production compared to other sources. This includes the most detailed chemical speciation of complex organic mixtures, obtained using both a high-resolution quadrupole time-of-flight mass spectrometer (MS) with soft ionization atmospheric pressure chemical ionization quadrupole time of flight (APCI-TOF) and a traditional vacuum electron ionization MS (EI-MS) both coupled to a thermal desorption system and a gas chromatograph (TD-GC). We leverage this detailed speciation to calculate the corresponding potential SOA production using literature SOA yields specific to carbon number and compound class, similar to previous work (*1*, *44*).

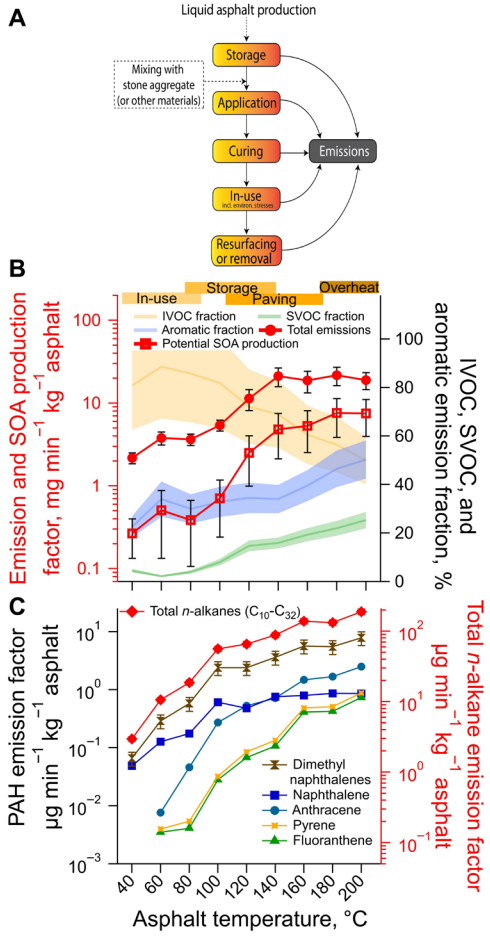

Fig. 1. Asphalt's life cycle and temperature-dependent emissions. (**A**) Different stages in asphalt's life cycle with potential to emit reactive organic gases into the atmosphere. (**B**) Temperature dependence of total gas-phase emissions from asphalt, ranging from in-use (40° to 60°C) and storage (80° to 140°C) to paving and overheating (120° to 200°C) temperature conditions (filled circles). The corresponding potential SOA that could be produced is also shown (hollow squares). The orange, green, and blue curves show the IVOC, SVOC, and aromatic fractions of the total emissions, respectively. The error bars indicate SD of the emission and SOA production factors, and the error bands indicate the SD in the volatility fractions. (**C**) Variation in the emission factors of select hazardous PAHs and total *n*-alkanes (C_{10}-C_{32}) with applied temperature.

RESULTS

Temperature dependence of asphalt-related emissions

Asphalt at typical application and in-use temperatures emits a complex mixture of organic compounds that span a wide volatility range. We subjected commonly used road asphalt collected during paving operations (i.e., pavement with aggregate and PG 64-22 binder) to a range of temperatures (40° to 200°C) in a temperature-controlled tube furnace supplied with purified "zero" air. New pieces of real-world road asphalt were used at each temperature step, and emissions were measured immediately once at set point temperatures with triplicates at each experimental condition to constrain sample-to-sample variability.

The total emission factor for primary road asphalt rose with temperature (Fig. 1B). It doubled from 40°C to 60°C (typical in-use summertime temperatures) and increased by 70% on average per 20°C temperature steps across 60° to 140°C (i.e., storage and application temperatures). Temperature also had marked effects on the volatility distribution of emissions, and changes with temperature were compound dependent (Fig. 1C). The IVOC fraction of total emissions decreased from 80 ± 18% (at 40°C) to 47 ± 10% (at 200°C), while the SVOC fraction increased from 4 ± 1% to 27 ± 4% over the same temperatures (Fig. 1B), and the remaining fraction largely composed of C_{10}-C_{11} VOCs. Contributions from VOCs smaller than C_{10} were negligible based on data from both GC-TOF and GC-EI-MS (fig. S1), although minor contributions of select VOCs (e.g., benzene, toluene, and C_{8-9} aromatics) were observed at the overspecification temperatures, likely as degradation by-products. The observed flattening of total emissions at highest temperatures may be influenced by decreased internal mass transport limitations because diffusion coefficients show relatively minor changes at higher temperatures (e.g., 140° to 200°C) compared to lower temperatures (e.g., 40° to 140°C) (fig. S2B).

Resolving the emitted complex organic mixtures

Using soft ionization high-resolution MS aided by GC separation, we chemically speciated the complex mixture of emissions from asphalt to a degree that had not been previously possible. This fully revealed the complexity and diversity of asphalt-related emissions in terms of molecular structures, heteroatom-containing compound classes, and volatility, all of which vary with emission conditions. A

wide range of aliphatic and aromatic structural features was observed and delineated according to molecular formulas (e.g., carbon number and number of rings or C═C double bonds). The aromatic fraction was relatively consistent (36 ± 8%) as emission factors increased with temperature. Aromatic emissions were comprised of single-ring compounds and PAHs (e.g., figs. S3 and S4), with their relative contributions varying with temperature from 85 to 55% and 15 to 45%, respectively, over 40° to 200°C. More broadly, PAHs made up 10 ± 6% of the total emissions and included known hazardous compounds such as anthracene, naphthalene, dimethylnaphthalene, pyrene, and fluoranthene, all of which increased with temperature (Fig. 1C, observed via GC-EI-MS). Similarly, tetralin and many isomers of methyltetralin, dimethyltetralin, tetramethylnaphthalene, methyl- and dimethyl-biphenyls, and dimethylbenzothiophene were also observed.

Figure 2 shows complex mixtures emitted at in-use (60°C) and paving/storage (140°C) temperatures speciated by their chemical formulas and displayed as a function of carbon number (i.e., volatility) and compound class. At all temperatures, emissions included a mix of straight and branched alkanes (average, 27 ± 8%), cyclic alkanes (average, 41 ± 3%; including mono-, bi-, and tri-cyclic compounds), single-ring aromatics (24 ± 3%), and PAHs (8 ± 5%). Hydrocarbons (i.e., compounds with C_xH_y formulas) constituted a greater fraction of total emissions, from 94% at 40°C, down to 56% at 200°C. Yet, sulfur- and oxygen-containing compounds (i.e., C_xH_yS and C_xH_yO formulas) contributed 1 to 14% and 5 to 30%, respectively, comprising a greater fraction of emissions at higher temperatures (fig. S5). Sulfur-containing emissions had the highest aromatic content (86 ± 2%) followed by oxygen-containing compounds (42 ± 5%) and hydrocarbons (30 ± 8%).

Sulfur-containing compounds were predominantly IVOCs and SVOCs (>80%), a quarter of which were PAHs, while oxygen-containing compounds were considerably higher in volatility (Fig. 2). Their volatility distributions were temperature dependent and showed significant increases in SVOC content at higher temperatures (Fig. 2). The fraction of SVOCs in sulfur- and oxygen-containing emissions increased with temperature from 12 to 50% and 5 to 13%, respectively, similar to the 4 to 28% increase in hydrocarbon SVOC content from 40° to 200°C, whereas relatively minor changes were observed in the overall distribution of compound types (e.g., aromatic versus aliphatic content) with changes in temperature (Fig. 2).

The highly aromatic sulfur-containing compound emissions include formulas representing benzothiophenes and dibenzothiophenes, a selection of which have been previously observed as individual compounds (fig. S6) (*45*, *46*). However, previous studies have not reported the wide range of other aromatic and non-aromatic sulfur-containing compounds in asphalt-related emissions. The complex mixture of oxygen-containing compounds includes formulas representing benzofurans and dibenzofurans that are often observed in complex petroleum-related mixtures (*47*). Yet, GC-TOF formulas and GC-EI-MS analysis demonstrate the presence of a wide range of thiophenes, carbonyls, aldehydes, and acids (fig. S6). For comparison, replicate tests in high-purity N_2 (5.0 grade) were conducted for

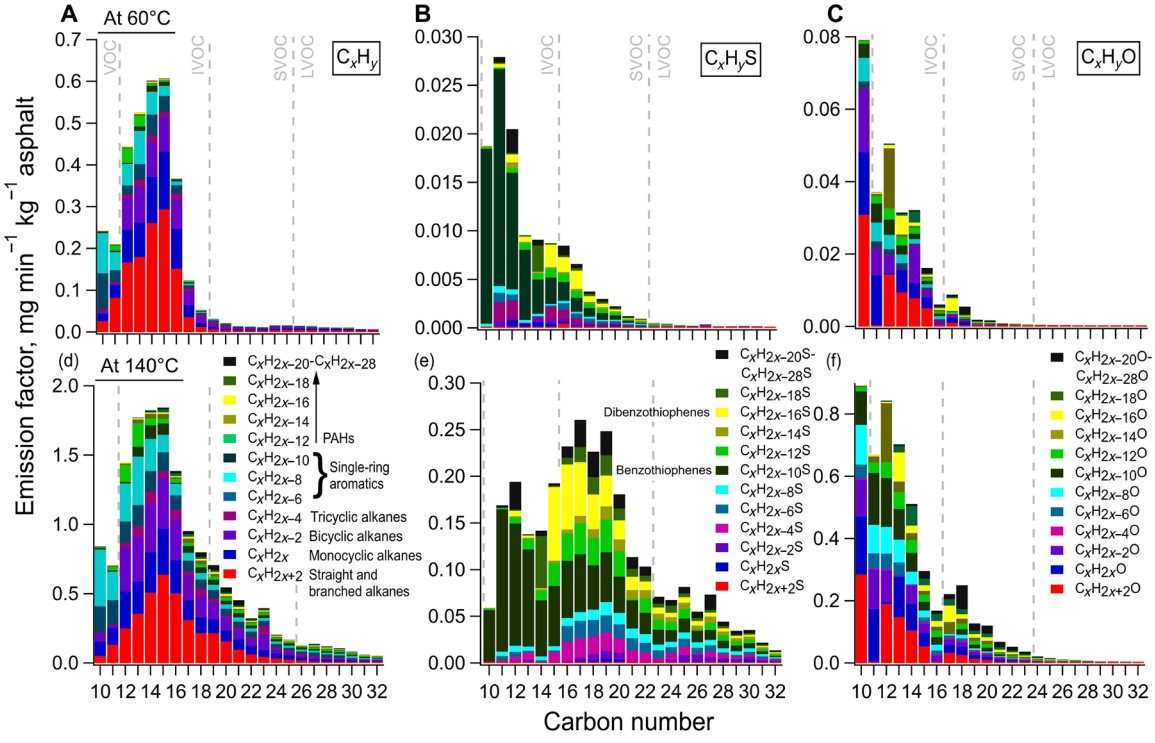

Fig. 2. Detailed chemical composition of hydrocarbons and functionalized organic compound emissions. Laboratory test results of the chemical composition of gas-phase complex mixture emissions from PG 64-22 road asphalt at typical in-use (60°C) and paving (140°C) temperatures. The emission factors and volatility distributions are shown in (**A**) and (**D**) for the hydrocarbon (C_xH_y) emissions, (**B**) and (**E**) for sulfur-containing compound (C_xH_yS) emissions, and (**C**) and (**F**) for oxygen-containing compound (C_xH_yO) emissions. The legend indicates distribution of molecular structures within each carbon number bin ranging from *n*-alkanes to PAHs. The trace signals on PAHs with formulas C_xH_{2x-20}-C_xH_{2x-28} (and corresponding heteroatom-containing formulas) are lumped together and labeled in black.

comparison to zero air and oxygen-containing emissions decreased substantially. They were almost negligible in tests conducted in N_2 but considerably enhanced in the presence of O_2 (in air), suggesting that they may be formed and not directly off-gassed from an existing volatile reservoir.

The calculated SOA production factor (see Materials and Methods and section S11) for primary road asphalt, enabled by our novel complex mixture speciation methods, increased with temperature's influence on total emissions and had an average SOA yield of 0.23 ± 0.09 (Fig. 1B), with greater SOA yields at storage and application temperatures (fig. S5). Hydrocarbons were dominant contributors to SOA production from asphalt-related emissions (73 ± 12% on average). The remaining SOA was equally produced from sulfur-containing (12 ± 8%) and oxygen-containing (12 ± 3%) compounds. In terms of volatility, IVOCs produced up to a maximum of 61% SOA at 60°C before gradually declining to 25% at 200°C, while contributions from SVOCs consistently increased from 12% at 60°C to 45% at 200°C, with the remaining 30% of SOA originating from LVOCs at the highest temperature (i.e., 200°C).

Changes in temperature-related emissions over time

Asphalt-related emissions changed considerably in magnitude and composition over time (Fig. 3 and fig. S7). To evaluate temporal dynamics and cumulative potential emissions, we subjected primary road asphalt (with PG 64-22 binder) to sustained heating at summertime in-use (60°C) and storage/paving (140°C) temperatures for multiple days (sections S4 and S6). In both cases, total emissions declined exponentially over time (Fig. 3, A and B, see equations), but emission rate dynamics varied between hydrocarbons and sulfur- and oxygen-containing compounds (fig. S7, A and B). Moreover, the volatility distributions began to shift after 1+ days of heating (fig. S7, C and D). Yet, the corresponding calculated SOA production followed the exponential decay in total emissions over time in both cases.

At 140°C, emissions of oxygen-containing compounds decreased more slowly followed by hydrocarbons and sulfur-containing compounds (fig. S7). The hydrocarbon fraction in total emissions at 140°C decreased from 71 to 40% over the first day of heating, while the oxygen-containing compounds increased from 17 to 56% and sulfur-containing compounds decreased from 12 to 4%. Yet, the production of oxygen-containing compounds decreased over longer time scales such that, 4 days later, mainly hydrocarbons remained (>91%) with minor contributions from oxygen-containing (~6%) and sulfur-containing (<3%) compounds. The fraction of single-ring aromatics remained relatively constant over the experiment. The volatility distribution of emissions changed over the first day of heating as the I/SVOC fraction decreased from 85 to 65% and then increased to a relatively stable 75 ± 8% during the remaining experiment (fig. S8). After 7 days at 140°C, emissions decreased to negligible levels, with total cumulative emissions reaching 30 g kg^{-1} asphalt.

Temporal emissions at 60°C had some marked differences compared to 140°C. Cumulative emissions over the course of the experiment were smaller at 1 g kg^{-1} asphalt. However, despite a faster decay rate than 140°C, the asphalt reached equilibrium with continued emissions at 60°C (0.1 mg min^{-1} kg^{-1} asphalt), exhibiting its potential as a long-lasting source of emissions in real-world environmental conditions beyond the 3 days tested here. While smaller in magnitude, emissions of oxygen- and sulfur-containing compounds did not have clear exponential trends, and sulfur emissions were more sustained than those containing oxygen (fig. S7A).

Increased emissions from asphalt upon solar irradiance

The vast majority of asphalt is used outdoors, where solar radiation represents a major environmental factor. To evaluate the effect of solar flux on asphalt-related emissions, we subjected our real-world road asphalt samples to solar spectrum radiation, including ultraviolet A (UVA) and UVB wavelengths, in the same quartz tube chamber housed in a temperature-controlled furnace and supplied with zero air. Representative conditions were used where the artificial solar flux on the samples was set up such that the exposure was similar to, or lower than, typical conditions. The artificial solar irradiance in our experiments was calculated to be 50% of the peak solar irradiance at mid-latitudes of the Earth's surface, thus allowing for a conservative emission estimate with higher emissions possible in cloudless conditions with full summertime sun exposure. Asphalt material temperatures were repeatedly measured, and heating was adjusted to ensure that the combined effect of temperature and applied solar radiation simulated summertime in-use conditions consistent with the temperature-only experiments (e.g., at 60°C). Emissions from primary road asphalt were measured over a period of 18 hours of constant solar exposure at 60°C starting with a measurement without solar exposure for comparison.

We found that solar exposure resulted in a nearly 300% increase in total emissions from road asphalt between the first two samples collected back-to-back without and with artificial sunlight (Fig. 3C and fig. S3). Sulfur-containing compounds showed the greatest increase (700%) followed by oxygen-containing compounds (400%) and hydrocarbons (300%). In all, heteroatom-containing emissions constituted 10% of total emissions under solar exposure, slightly higher than 7% in its absence. Total emissions declined with time but exhibited a much slower, nonexponential decay rate than the exponential drop observed in temperature-only experiments. The total emissions measured at the 18th hour were still 30% higher than the first sample collected at the 0th hour without artificial sunlight (Fig. 3C), whereas in the temperature-only experiments, they had reduced to ~10% of the initial emission factor after 18 hours of heating (Fig. 3A).

The volatility distribution of emissions was highly sensitive to solar exposure (Figs. 3, C and D, 4). Initially, emissions from road asphalt (Fig. 3C) were composed of 80% IVOCs, but the volatility spectrum shifted toward more SVOCs over time, with the IVOC fraction averaging 35 to 40% beyond the first 3 hours of solar exposure and the SVOC fraction going from <5% in the nonsolar sample to peaking at over 40% after 5 hours of exposure and producing a local maxima in emissions and SOA production. The aromatic fraction of the total emissions remained between 15 and 25% throughout the experiment, but the relative contributions of PAHs to total aromatic emissions increased from 20% in nonsolar conditions to a relatively stable 40 ± 3% during irradiation, implying an enhanced production of emittable PAHs under solar exposure (fig. S4).

Unlike the extended temperature-only experiments (i.e., Fig. 3), the calculated SOA production factor remained high during sustained solar exposure. Despite a decrease in total emissions after initial solar exposure, it increased to a maximum of 5 mg min^{-1} kg^{-1} asphalt after 5 hours of irradiance and was consistently elevated throughout the 18-hour experiment (Fig. 3C). The SOA yield increased from 0.11 in nonsolar conditions to 0.21 initially with solar exposure and

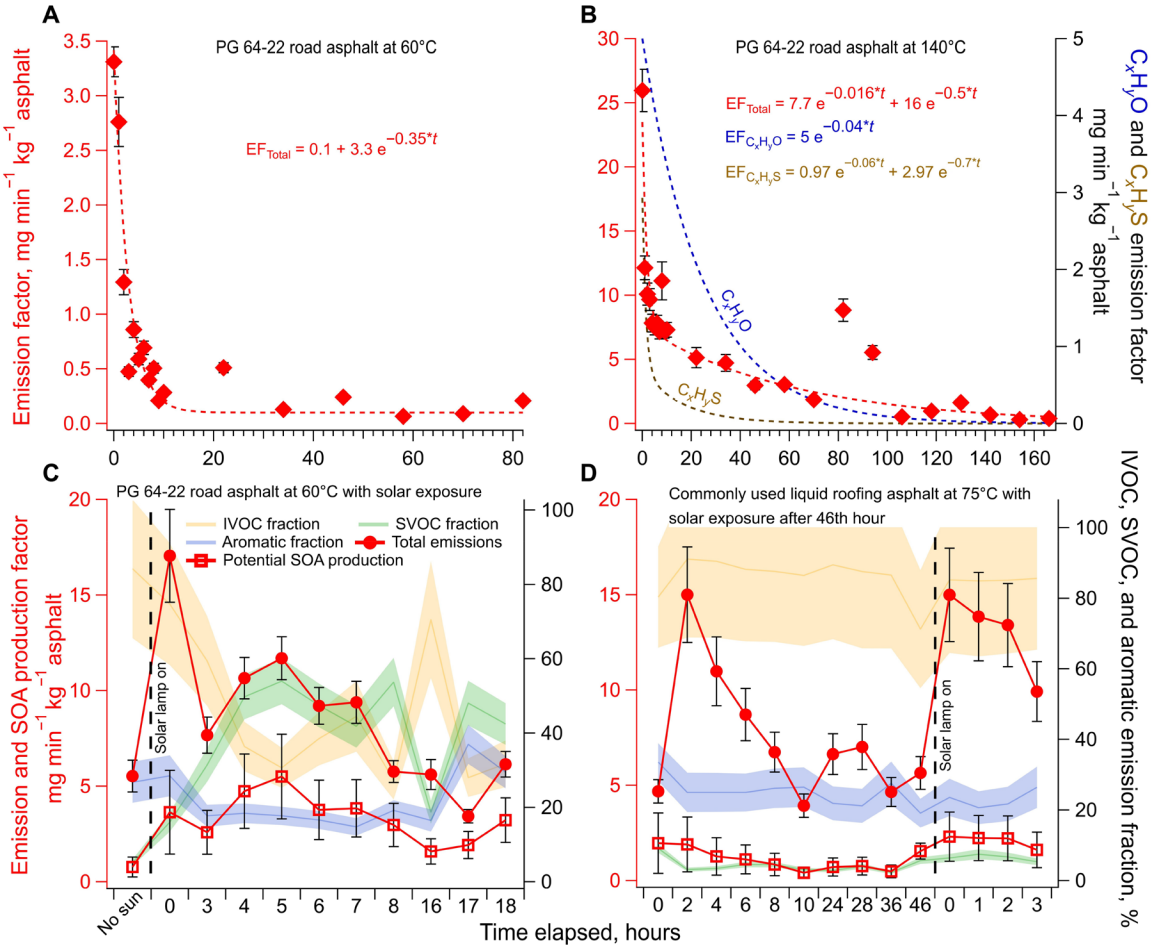

Fig. 3. Changes in temperature-related emissions over prolonged heating and large emission enhancements with solar exposure. (**A** and **B**) Variation in total gas-phase emission factors over time from commonly used PG 64-22 road asphalt as observed in laboratory experiments simulating (A) in-use temperatures (60°C) and (B) paving temperatures (140°C). Individual markers for the C_xH_yS and C_xH_yO fitted decay curves in (B) are shown in fig. S7, including for 60°C where heteroatom-containing emissions were minor and did not exhibit a clear decaying trend. Additional details including SDs on equations in (A) and (B) can also be found in fig. S7. (**C** and **D**) Emission enhancements due to solar exposure shown with total gas-phase emission factors (solid circles) and SOA production factors (hollow squares) over time for (C) PG 64-22 road asphalt under solar exposure at 60°C and (D) commonly used liquid roofing asphalt under solar exposure at 75°C. The orange, green, and blue curves in both panels show the IVOC, SVOC, and aromatic fractions of the total emissions, respectively, and are shown as a function of discrete time points on the *x* axes. The error bars and error bands indicate SD in emission factors and SOA production factors, respectively. Emissions from liquid roofing asphalt exclude any potential contributions from Stoddard solvent off-gassing.

then to a relatively stable 0.44 ± 0.09 throughout the remainder of the experiment. This increased SOA yield and sustained potential SOA production was the result of the clear enhancement in SVOCs (that increased over the first few hours of solar exposure) and continued production of both IVOC and SVOC emissions with irradiance (Figs. 3C and 4).

Ozone exposure (without artificial sunlight) was also tested as an environmental stress that leads to degradation-related emissions from some products/materials (*1*). However, asphalt-related emissions did not exhibit any sensitivity toward a range of ambient ozone concentrations [50 to 100 parts per billion (ppb)] in terms of total emissions or chemical speciation, showing minimum capacity for ozone-related emissions and suggesting minor amounts of unsaturated non-aromatic compounds in its emissions (e.g., alkenes).

We conducted similar solar exposure experiments with liquid asphalt used in roofing and pavement sealing applications with the dual objectives of investigating (i) reactive organic emissions from roofing asphalt and (ii) temperature versus solar-related emissions from asphalt binder (without the presence of aggregates). A thin layer of viscous liquid asphalt was held at 75°C (a typical summertime maxima attained by asphalt-coated roofs; see section S2) (*48*) for 46 hours to decrease temperature-driven emission pathways and/or reservoirs before the solar lamp was turned on (fig. S11). Total emissions declined over time during the heating-only period, consistent with previous observations under constant temperature, followed by a 260% increase with solar irradiance (relative to 46th hour emissions; Fig. 3D). This included increases in hydrocarbons (250%), sulfur-containing compounds (500%), and oxygen-containing compounds (400%), although the latter two contributed less than 4% to total emissions. Yet, these observations from both road and liquid asphalt indicate that artificial solar radiation produced enhancements in oxygen/sulfur-containing emissions, which are otherwise lower at in-use temperatures. This sharp increase in emission after ~2 days of heating demonstrates a solar irradiation–activated

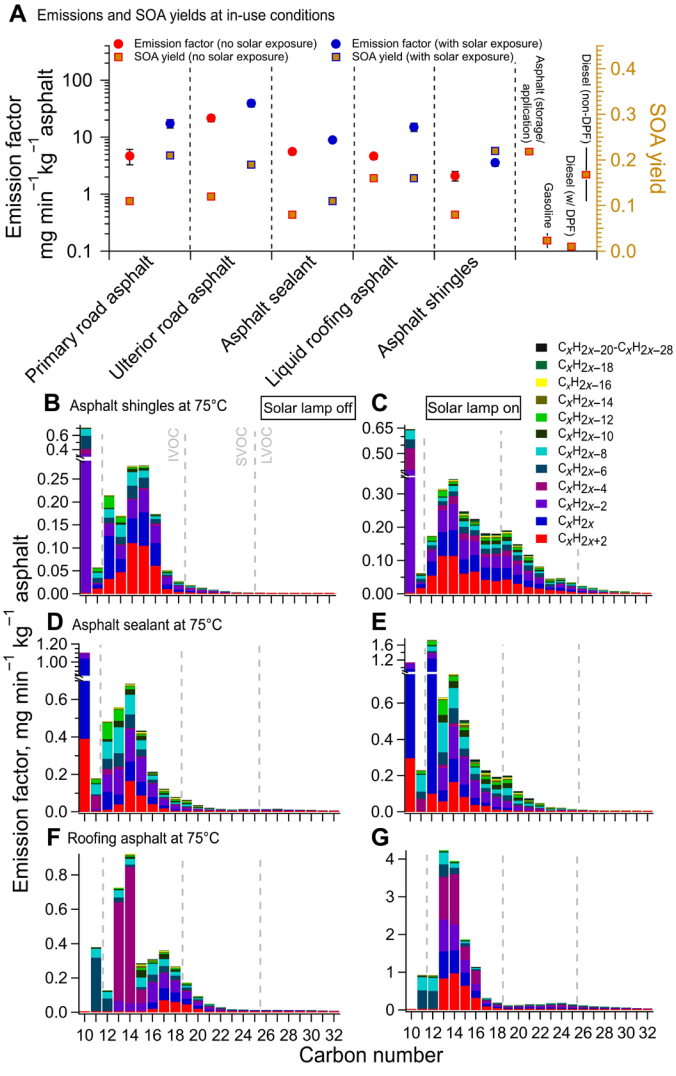

Fig. 4. Other asphalt-containing materials have similar emissions and solar enhancements. (**A**) Summary of emission factors and SOA yields for different highly used asphalt-based materials compared to gasoline and diesel emissions. The red circles and red-bordered squares indicate emission factors and SOA yields, respectively, determined in the absence of solar exposure, while the blue circles and blue-bordered squares show the corresponding values measured with the material exposed to solar radiation. Variation in chemical speciation of hydrocarbon (C_xH_y) emissions observed during laboratory tests without (left) and with (right) sunlight are shown in (**B**) and (**C**) for asphalt shingles at 75°C, (**D**) and (**E**) for asphalt-based sealant at 75°C, and (**F**) and (**G**) for commonly used liquid roofing asphalt at 75°C. Hydrocarbon emissions made up more than 80% of total emissions in most cases.

emission pathway that is independent of temperature-related emissions at in-use temperatures. The IVOC fraction started and remained high (85%), the SVOC fraction increased from 3 to 9%, and the aromatic fraction was similar to nonsolar conditions (Fig. 3D), but the PAH fraction did not shift like with road asphalt.

Emissions from other common road and roofing asphalt-based materials

In addition to our detailed testing of primary road asphalt (PG 64-22 binder), we observed emissions of complex mixtures of hydrocarbons and heteroatom-containing compounds across the VOC-I/SVOC range from three widely used, commercially available, asphalt-containing roofing products, specifically asphalt shingles, asphalt sealant, and liquid roofing asphalt. All roofing materials were tested immediately after heating to 75°C, which is a typical maximum for roof surfaces (*42*), slightly higher than road surface maxima (see section S2). All the asphalt-containing products/materials emitted complex mixtures of IVOCs, SVOCs, and C_{10}-C_{11} VOCs with 20 to 50% aromatic content (Fig. 4, B, D, and F) and a range of comparable emission factors (Fig. 4A). It should also be noted that the use of solvents in some of these products such as sealants (i.e., light aromatic solvent) and liquid roofing asphalt (i.e., Stoddard solvent with C_9-C_{12} aliphatics) could further increase their emissions and SOA formation potential. For comparison here and to focus on the non–solvent-related emissions, high-resolution formulas for any potential contributions from solvents are conservatively excluded from measured emissions.

These asphalt-containing materials showed substantial increases in total emissions, I/SVOC emissions, calculated SOA yields, and thus SOA production with solar irradiation at or below typical solar fluxes (Fig. 4A). Figure 4 (C, E, and G) shows the distribution of hydrocarbon emissions with solar irradiation, which constituted the majority of emissions from asphalt shingles (85%), asphalt sealant (80%), and liquid roofing asphalt (78%) at 75°C, with the remainder constituted by sulfur- and oxygen-containing compounds. It is worth noting that the increases in the fraction of SVOC emissions due to solar exposure were somewhat more pronounced for asphalt shingles and both road asphalts (Fig. 4 and fig. S3) compared to asphalt sealant and liquid roofing asphalt. This relative enhancement was also reflected in their SOA yields, yet the only known difference was the presence of coarse (e.g., road asphalt) or fine (e.g., asphalt shingles) stone aggregates.

To further supplement the extensive testing of primary road asphalt from New Haven, CT, with PG 64-22 binder, which is very common throughout the United States and California, we tested an additional real-world sample of road asphalt from Pittsburgh, PA. A large specimen of road asphalt pavement was collected approximately 28 hours after application in Pittsburgh, PA, from an ulterior (i.e., minor) road using a different binder grade. We tested it at 40° and 60°C in the laboratory to examine emissions at daily in-use temperatures (Fig. 5). The total emission factors were five to seven times higher than from primary road asphalt at 60° and 40°C, respectively, even considering that it had been paved over 1 day before the pavement sample was obtained.

A similar hydrocarbon volatility distribution was observed between the Pittsburgh ulterior road asphalt (Fig. 5B) and the primary road asphalt (Fig. 2A). Similar to the New Haven primary road asphalt, hydrocarbons made up over 95% of the emissions from the Pittsburgh sample at 40° to 60°C, with the remaining being a combination of sulfur- and oxygen-containing hydrocarbons. The total emissions were largely IVOCs (73%), with SVOCs making up only 4%. Nearly 37% of these emissions were aromatic at both 40° and 60°C, constituted by single-ring aromatics (95%) and PAHs (5%). The SOA yields for emissions at 40° and 60°C were comparable between the two road asphalt types, and both materials showed significant enhancements in SOA yield with solar exposure (Fig. 4A). These results demonstrate that (i) emission factors (with and without sunlight) for a road asphalt specimen collected from a different region and road type are variable and can be substantially greater than the primary road asphalt sample

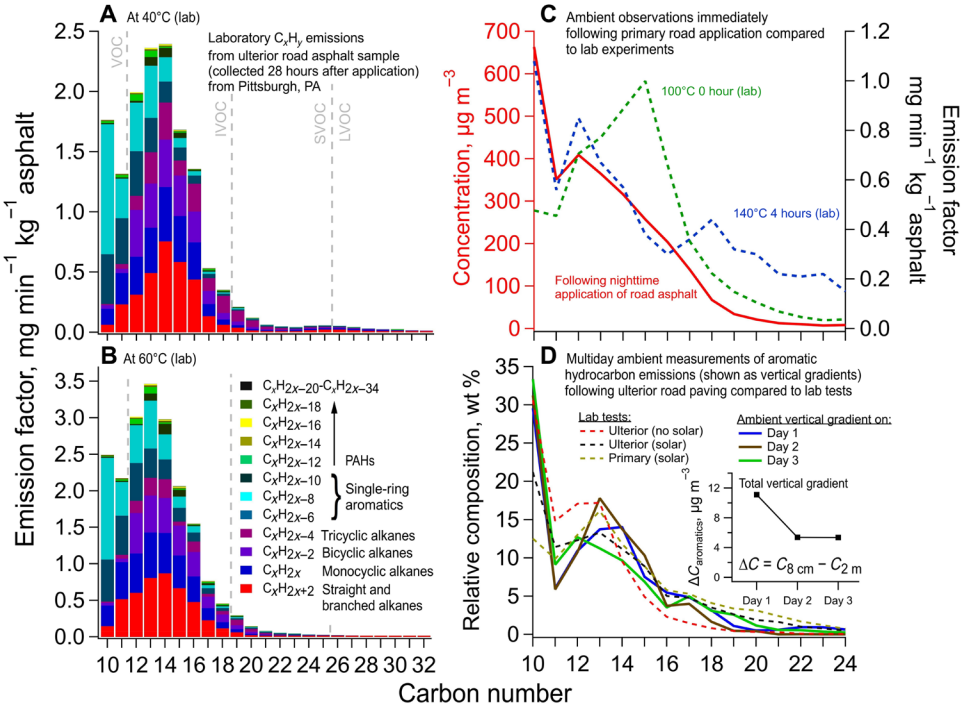

Fig. 5. Consistent results from other asphalt samples and ambient measurements. (**A** and **B**) Chemical speciation of complex gas-phase hydrocarbon emissions from ulterior (i.e., minor) road asphalt collected from Pittsburgh, PA, during laboratory tests at (A) 40°C and (B) 60°C. In both cases, hydrocarbons made up over 95% of the total emissions. (**C** and **D**) Confirmatory ambient measurements following road asphalt application demonstrate similar emissions (shown as a function of carbon number) for (C) primary roadway asphalt immediately following application in New Haven, CT (detailed composition in fig. S9) and (D) over 3 days of measurements at an ulterior roadway in Pittsburgh, PA, both compared to laboratory experiments. To evaluate continued vertical fluxes (i.e., emissions) over 3 days, the main plot in (D) shows the aromatic vertical concentration differentials at 8 cm versus 2 m (i.e., Conc. at 8 cm − Conc. at 2 m) via simultaneous adsorbent tube collection at the 2 heights. Single-ring aromatics and PAHs are shown here to remove biogenic interferences, but supporting vertical gradient data via GC-TOF and GC-EI-MS for alkanes, aromatics, and PAHs can be found in figs. S9 and S10. The inset in (D) shows the sum of vertical concentration differential for aromatic compounds. The field results from the 3 days show good agreement with laboratory data, including SVOC enhancements with solar exposure.

tested in this study, (ii) the chemical composition of emissions is similar, and (iii) there are large continued emissions (observed in laboratory) at in-use conditions even 1 day after curing of real-world asphalt.

Observations from supporting ambient measurements

To supplement the extensive laboratory-based results presented here, we collected a selection of targeted ambient field samples that provide evidence for real-world emissions of aromatic and aliphatic I/SVOCs following road asphalt application over a range of time scales at two separate sites. First, three ambient nighttime samples were collected on adsorbent tubes in the period immediately following primary road asphalt application (section S3). These results from freshly applied road asphalt during cooling (Fig. 5C) show a wide volatility range generally consistent with laboratory results. Specifically, the distribution of smaller compounds is more consistent with that observed in laboratory experiments at 140°C after several hours of heating (fig. S7D), while the relative abundances of larger compounds are more consistent with tests at 80° to 120°C as the asphalt cools (Fig. 5C).

Second, daytime samples collected over 3 days at an ulterior roadway site demonstrate sustained emissions at ambient temperatures of 25° to 35°C (Fig. 5D and figs. S9A and S10). They had a similar volatility distribution to that of the laboratory tests of the ulterior roadway asphalt pavement sample (taken from that site), shown with and without solar exposure in Fig. 5D. Each day at a similar time in the afternoon, simultaneous gas-phase VOC-I/SVOC samples were collected at 8 cm and 2 m above ground level to evaluate vertical concentration gradients resulting from emissions at the asphalt surface. Such gradients are frequently used to investigate vertical fluxes from ground-level sources (*49*). The concentration differential in the vertical gradient between the two heights demonstrated the upward vertical flux of VOCs-I/SVOCs, independently in both GC-TOF (Fig. 5D and fig. S9) and GC-EI-MS (fig. S10) data. These apparent emissions continued over the 3 days of measurements with similar vertical concentration gradients on days 2 and 3 after a 50% decrease from day 1 (i.e., the day of application) (Fig. 5D, inset).

All 3 days were sunny at the site and the observed vertical fluxes of aromatics included a distribution of larger C_{15}-C_{20} compounds that was more consistent with the solar-exposed experiments than the temperature-only experiments or nighttime ambient observations (Fig. 5, C and D). PAHs and single-ring aromatics are shown in Fig. 5D to minimize interferences from evident biogenic emissions of terpenoid species and previously reported alkanes [e.g., even *n*-alkanes (*50*)] at the heavily vegetated site. Yet, there is evidence for vertical gradients in asphalt-derived alkanes that are concentrated in the IVOC range (figs. S9 and S10), with a breakdown similar to laboratory data. Both sets of these real-world observations are intended to support the conclusions of the laboratory experiments, yet future work remains for more detailed field measurements

across a broader range of asphalt life cycle stages with quantitative flux measurements (e.g., eddy covariance) over longer time periods.

DISCUSSION

Constraining emissions of intermediate- and semivolatile SOA precursors from asphalt-related materials

The magnitude and composition of emissions from asphalt-based materials are dependent on environmental conditions, particularly temperature and solar radiation, often with the vast majority of emissions composed of I/SVOCs. During our tests, substantial emissions were observed in response to these stresses, with an experimental focus on emissions from road asphalt during application and the initial period thereafter. Here, we use these results on road and roofing asphalt to conservatively estimate the range of potential total emissions from asphalt-related materials and to ultimately contextualize their importance for urban air quality in the subsequent section.

Emission factors decayed over the tested time scales (up to 1 week), yet had continued emissions at in-use temperatures (e.g., 60°C) and especially with solar exposure (Fig. 3). To translate these results to potential emissions during the application and in-use life cycle stages, we established lower and conservative upper estimates using both the initial emission factors for all the asphalt materials tested and calculated the total emissions observed during the prolonged experiments. Given the variability in asphalt types and environmental conditions (discussed below), this provides an approach to constrain larger-scale emissions and is further detailed in section S8 (see the Supplementary Materials).

Temperature-related emissions from road asphalt

To determine the temperature-driven emissions capacity (i.e., the total possible emissions with perpetual heating) from the real-world primary road asphalt (i.e., Fig. 3B), we continuously heated an asphalt pavement sample to application temperatures (140°C) for 1 week until emissions were negligible. We observed a total of 30 g of total emissions per kilogram of primary road asphalt binder (PG 64-22 grade), which was estimated via the emissions decay curve fitted to time-dependent EF measurements (Fig. 3A and section S8). Yet, higher total emissions are possible with other road asphalt grades as evidenced by the higher EFs measured from Pittsburgh's ulterior road asphalt (Fig. 5). Fourteen percent of the potential total emissions (i.e., 14% of 30 g kg^{-1}) were emitted in the first 5 hours of heating, an approximate period during which road asphalt remains at high temperatures while in transport from storage and during subsequent paving. Therefore, despite longer possible heating times, only 14% of the potential total emissions were considered in reporting potential emissions from road asphalt while at application conditions (Table 1), and future on-site ambient measurements during and following application via different methods are warranted to further constrain the full extent of application-related emissions.

Some fraction of the remaining temperature-driven emittable content (26 g kg^{-1}) could slowly diffuse out from the cured road asphalt over time, especially at higher in-use summertime temperatures (e.g., 60°C). To conservatively estimate potential emissions at in-use conditions, Table 1 only reports in-use emissions from the 60°C experiments over the ~3 days tested, which amounted to 1 g kg^{-1}, and could be higher by a factor of 5 based on the ulterior road asphalt sample (Fig. 4). However, emissions were not depleted during the experiment, reaching a steady-state emission rate of 0.1 mg min^{-1} kg^{-1} (Fig. 3A) that was limited by internal diffusion (see section S7). Thus, steady-state emissions extending beyond the duration of the experiment were not included in Table 1, and it should be noted that these steady-state emissions would equate to an additional 1 g kg^{-1} over another 7 days at 60°C.

In addition, emissions during production/processing and from distributed storage facilities, which keep asphalt binder at hot temperatures, are not included in Table 1's estimates. Yet, these I/SVOC emissions are likely occurring and represent another key area of future work as the vast majority of asphalt-related emissions from all life cycle stages are outside the range of traditionally used VOC measurement techniques [e.g., Photochemical Assessment Monitoring Stations (PAMS) network].

Solar exposure–related emissions from road asphalt

Solar radiation markedly increased emission factors for in-use road asphalt and decayed more slowly relative to temperature-related emissions (Figs. 3, C and D, and 4) such that the time scales for the depletion of sunlight-related emissions are uncertain. Therefore, to include a lower bound for the potential solar-related emissions in Table 1 for road asphalt, we have integrated emissions over the 18-hour experiment (Fig. 3C), which was conducted at only moderate solar fluxes (section S5 and fig. S11B). To account for differences in pavement thickness and only consider solar-related emissions from the asphalt pavement's surface, we have scaled down the results from our solar radiation experiments to represent the typical thickness when repaving with road asphalt (see section S8). Yet, we acknowledge that total emissions would likely be higher with additional solar exposure beyond 18 hours and with higher solar fluxes, such as on peak solar days or at lower latitudes. Therefore, to establish an upper estimate, we integrated the potential total emissions from the emissions decay curve fitted to the data, as described in section S8.

Roofing asphalt–related emissions

Asphalt-based roofing materials are exposed to both high temperatures and solar radiation. Potential temperature-related emissions were estimated on the basis of summertime black roof temperatures (75°C) using the time-resolved liquid roofing asphalt experiments (Fig. 3D), which had the median temperature–related EF for the roofing asphalt (section S8). The lower limit corresponds to total emissions over the experiment's duration (~2 days), while the upper limit is calculated via fitting and integrating an emissions decay curve to the time-dependent EFs (section S8). Solar exposure caused a significant enhancement in emissions for all roofing materials (Fig. 4), even after sustained heating (Fig. 3D). A lower bound based on our data is the sum of emissions over 3 hours of solar exposure during the experiment (Fig. 3D). The upper bound is conservatively estimated by assuming the decay rate to be similar to that for emissions without solar exposure.

Emission reservoirs and potential production pathways

The underlying reservoirs and processes related to emissions of the diverse mix of observed compounds are discussed here based on our results, but opportunities remain for further elucidation. First, the fraction of hydrocarbon emissions (relative to functionalized organic compounds) from both road and roofing asphalts were greater at lower temperatures (Fig. 2 and fig. S5), suggesting that at least some fraction of hydrocarbon compounds or their precursors are in a more readily accessible reservoirs in asphalt, whereas sulfur- and oxygen-containing compounds are dependent upon emission pathways that require higher temperatures to overcome formation or mass transport limitations.

Table 1. Emissions and potential SOA estimates for asphalt-related materials and pathways in comparison to other prominent sources in the South Coast Air Basin (SoCAB), California. Asphalt-related emissions from upstream production, transport, and distributed storage before application are not included and would increase cumulative life cycle emissions. Please see section S8 for details on calculation of individual values. *Includes hot- and warm-mix asphalts but excludes emulsified and cutback asphalt (8% of total usage), which are applied cold. †Corresponds to PG 64-22 road asphalt, which represents common road asphalt in California. Higher emissions are possible due to losses before collection of asphalt. Other asphalt types may have higher application emissions, e.g., the Pittsburgh sample with five times higher emissions at 60°C. ‡The potential SOA production at application temperatures includes LVOCs (and some larger SVOCs) that may recondense before undergoing atmospheric oxidation. §Includes emulsified and cutback asphalts (6 and 2%), which are applied cold. ‖Does not include emissions beyond the experiment duration, i.e., ~3.5 days. ¶Annual solar-related road asphalt emissions have been adjusted for the mass fraction exposed to solar light. #Does not include emissions from coal-tar pitch roofing products, which are likely a similar or greater source where used. **Only 5% of roofing asphalts are applied hot. ††Fuel consumption and on/off-road emissions calculated using California Air Resources Board EMFAC and OFFROAD 2017 models (*70*, *71*). Values correspond to the year 2020. ‡‡Includes both exhaust and evaporative emissions (i.e., from vehicles and fuel distribution) (*72*). §§Known I/SVOC emissions from VCPs are concentrated largely in the lightest IVOC C* bin in the study of McDonald *et al.* (*2*). VCP estimates shown here do not include asphalt-related contributions from this study.

Asphalt emission pathway or source type	Usage in California (Tg/year)	Usage in SoCAB (Tg/year)	Potential emissions (g/kg product)	Potential I/SVOC emissions (g/kg product)	Potential SOA (g/kg product)	SoCAB annual average I/SVOC emissions (Gg/year)	SoCAB annual average potential SOA (Gg/year)
Road asphalt application (e.g., 140°C)*	1.11	0.5	≥4.1†	≥2.9	≥0.9‡	≥1.4	≥0.45
Road asphalt in-use (e.g., 60°C)§	1.22	0.55	1.0–5.0‖	0.8–4.1	0.1–0.5	0.4–2.3	0.1–0.3
Road asphalt in-use under solar irradiance¶	1.22	0.55	2.1–5.5	1.8–4.6	0.4–1.2	1–2.5	0.2–0.6
Liquid roofing asphalt hot application (e.g., 140°C)#	0.009**	0.004	≥4.1	≥2.9	≥1.1	≥0.01	≥0.004
Roofing asphalt in-use (e.g., 75°C)	0.183	0.083	18–43	16–39	2.8–6.9	1.3–3.2	0.2–0.6
Roofing asphalt under solar irradiance	0.183	0.083	2.1–42	1.9–38	0.3–7	0.2–3.2	0.02–0.6
Asphalt total	1.4	0.63	–	–	–	4.3–12.6	1–2.5
Gasoline-related sources (2020)	44††	18.1††	1.7‡‡	0.05–0.2	0.03–0.04	0.9–2.9	0.5–0.7
Diesel-related sources (2020)	16.4††	4.43††	0.72	0.4	0.08–0.2	1.7	0.4–0.7
Known VCPs	3.26	1.48	120 ± 30	24 ± 6‡‡	4.7 ± 1.7	35 ± 9§§	7.0 ± 2.5

Second, mass diffusion within the viscous asphalt binder is a rate-limiting factor for emissions. Road asphalt's EFs were an order of magnitude higher at 140°C than 60°C and decayed more slowly over time (Fig. 3, A and B), and relative changes in emission factors (Fig. 1) generally followed changes in internal diffusion coefficients (fig. S2, B to D). At higher temperatures, there is enhanced internal diffusion to the asphalt surface from internal reservoirs due to the lower viscosity of the asphalt binder, which will be 100 times greater at 140°C versus 60°C (see section S7). The results from prolonged heating at 140°C (Fig. 3B) further suggest complete depletion of both preexisting reservoirs and any temperature-related formation mechanisms (e.g., for S- and O-containing species). The other potential explanation could be pyrolysis of asphaltenes to produce VOCs-I/SVOCs but is unlikely because asphaltenes require very high temperatures (>200°C) to begin fragmenting (*51*, *52*).

Therefore, we hypothesize there are some preexisting reservoirs of VOCs, IVOCs, and SVOCs in asphalt from upstream operations, which diffuse out from cured asphalt over prolonged time scales at rates governed by binder viscosity, temperature, and film thickness (i.e., diffusion-path length). This is supported by the observed steady-state emissions during continuous heating at 60°C (Fig. 3A), mass transport calculations (see section S7), the correlation between *n*-alkane emission factors (Fig. 1C) and their calculated internal diffusion coefficients as a function of temperature (fig. S2, C and D), and the sharp decrease in EFs at 60°C due to the depletion of VOCs-I/SVOCs in the surface layer.

While emissions will be enhanced in hotter temperatures, this mass diffusion limitation suggests that the internal distribution of compounds will equilibrate during cooler periods via internal diffusion (albeit at slower diffusion time scales; section S7). This process would replenish near-surface reservoirs before future hot periods and the accompanying enhanced temperature-dependent partitioning at the surface, which would increase the in-use emission estimates in Table 1.

Third, separate VOC-I/SVOC production pathways become important with exposure to solar radiation. In our experiments, the application of solar radiation on both road and roofing asphalts showed immediate, sustained increases in total emissions (at the

same temperatures), even with solar exposure occurring after ~2 days of continuous heating (Figs. 3, C and D, and 4). Solar-related emissions eventually decreased but at a much slower rate than in temperature-only experiments (Fig. 3, A and B). Together, this evidence suggests enhanced production of emittable compounds via an independent pathway at a rate rivaling their temperature-only related emissions.

The exact mechanism(s) cannot be derived via the results of this study, but a potential hypothesis is that organic compounds (or segments of organic compounds) present in asphalt are acting as chromophores and generating triplet excited states of organic matter through photosensitization and/or singlet oxygen ($^1O_2$) through energy transfer to ground state oxygen (*53*). These reactive species may then react with larger less-volatile structures (e.g., asphaltenes) to form smaller, emittable compounds (*54*–*56*). Similar photoexcitation of chromophores is known to occur in atmospheric light-adsorbing brown carbon that undergo photoinitiated transformations over time—analogous to the photobleaching observed with real-world asphalt (*55*, *57*). Similarly, the generation of other reactive species (e.g., H_2O_2) via irradiation of quinone-like structures known to form from PAH oxidation could also play a role (*58*–*61*). Another possibility is direct photolysis of organic compounds excited via increased absorption in the UV-visible spectrum, which could be facilitated by the prevalent π-bond conjugations present in asphaltene molecules. In principle, C═C bonds could be broken by UVA and UVB radiation [bond energy, 348 kJ mol^{-1} or an equivalent wavelength (λ) of 344 nm] (*62*).

It is also worth noting that heavy metals such as copper, nickel, vanadium, zinc, and cadmium are present in asphalt binder along with a range of other metals and could be a factor in the observed photoactivated chemistry (*8*). However, more detailed investigation is necessary to explore these hypotheses using additional targeted instrumentation to examine the chemical functionality of surface layers following solar exposure. As part of this, future work should explore the role of individual solar wavelengths on the magnitude and chemical composition of emissions from asphalt while also examining the solar-enhanced emissions across a range of surface temperatures. Because the identity of the chromophores is unknown, their long-term stability and persistence is uncertain and can be explored in longer duration tests. For all these emission pathways, future work is needed to examine the effects of polymer-modified asphalts, other additives, porous asphalts, variations across other asphalt grades/products and application methods (e.g., hot-mix, warm-mix, or emulsified asphalts), and the effect of real-world road wear on potentially exposing new asphalt surface layers over time.

Comparing intermediate- and semivolatile emissions and SOA production to other urban sources

To evaluate the importance of asphalt-related emissions on urban scales, we assessed their relative contributions of SOA precursors including a focus on I/SVOCs given their established role in SOA production (*4*). We compared their emissions to known sources in the more developed California-based emission inventories and studies, especially the South Coast Air Basin (SoCAB), which is an important historical urban air quality case study (*1*, *2*). Road asphalt is responsible for 86 to 87% of total liquid asphalt binder used in California and the United States (fig. S12 and Table 1), with the remainder used primarily for roofing (*1*). The primary road asphalt binder tested in this study (PG 64-22 grade) or other very similar grades (PG 64-10 and PG 64-16) are prevalent in the SoCAB (*63*). Compared to other regions, there are fewer seasonal asphalt application restrictions, but increases in emissions due to higher surface temperatures and solar exposure will occur during the summertime air pollution season (June to August, 35° to 45°C high air temperatures, 870 W m^{-2} peak solar intensity). In colder climates, application-related emissions will be focused during warmer months when they will contribute most to SOA formation in urban areas.

Both our GC-TOF and GC-EI-MS results demonstrate that emissions contained a large fraction of I/SVOCs (C_{12}-C_{25}) in addition to VOC emissions in the C_{10}-C_{11} range (Figs. 2 to 5 and figs. S1 and S10), both of which have substantial aromatic content (30 to 40%). In general, asphalt-related emissions have a greater proportion of I/SVOC emissions than most other sources (Figs. 2 to 5), which, in turn, contributes to their large SOA yields (Fig. 4). Approximately 66 to 81% of emissions from primary road asphalt were I/SVOCs at both application and in-use temperatures. With solar radiation, the I/SVOC fraction of road asphalt (at 60°C) increased to 85% (fig. S13). The other asphalt materials tested had similarly large I/SVOC fractions ranging from 62 to 90% (Fig. 4 and fig. S13). By comparison, emissions from gasoline vehicles contain only a small fraction of gas-phase I/SVOCs (*64*), while the larger molecular sizes in diesel fuel lead to a I/SVOC fraction of 52% in total diesel emissions (section S8) (*65*). However, I/SVOC emissions, and thus SOA yields, have dropped markedly for modern diesel vehicles equipped with diesel particulate filters (DPFs) and diesel oxidation catalysts (DOCs) (*66*).

Given their high I/SVOC emission factor and the large quantity of asphalt used, total asphalt-related emission rates in the SoCAB exceed those of traditional combustion-based sources such as gasoline and diesel motor vehicles and individually contribute a substantial increase in I/SVOC emissions to those currently estimated for VCPs (Table 1). I/SVOC emissions from asphalt-related sources include large contributions from road asphalt application as well as temperature- and solar-related emissions from both road and roofing asphalts at in-use conditions (Table 1). Together, this makes asphalt-related materials a major source of I/SVOC emissions and a likely contributor to the large unattributed contributions of I/SVOCs from unknown petroleum-related sources (i.e., other than on-road motor vehicles) previously observed in ambient measurements in the SoCAB (*5*). Similar supporting ambient evidence from the SoCAB in 2010 shows an observed temperature dependence and an unexpected afternoon maxima in naphthalene and methylnaphthalene concentrations (observed here in asphalt-related emissions; e.g., Figs. 1, 2, and 5), which could not be differentiated between local emissions from the "tar roof" or a larger city-wide source in the study (*67*). In all, it reinforces the importance of targeted ambient measurements and long-term laboratory experiments simulating application and environmental conditions with typical perturbations across a greater geographic diversity of asphalt materials. This future work should aim to quantify emissions over the complete life cycle of asphalt, whose cumulative impacts on urban environments could increase beyond current estimates (e.g., Table 1) over longer time scales.

While the SOA production factor (g kg^{-1} asphalt use) from roofing asphalt materials is higher than that from road asphalt, road asphalt contributes a greater fraction to estimated potential SOA production in the SoCAB due to its higher consumption (Table 1). Solar radiation–related emissions have a large SOA production

potential due to their enhanced I/SVOC emissions and SOA yields such that their emissions from both road and roofing materials are likely responsible for approximately 30 to 50% of asphalt-related potential SOA. Given cities' substantial asphalt coverage, the major contributions of ambient temperature- and solar-related pathways to I/SVOC emissions (70 to 90%; Table 1) suggest a more spatio-temporally distributed urban source than emissions arising from application alone.

In total, the annual potential SOA production from asphalt-related sources in the SoCAB is greater than that of gasoline and diesel on-road motor vehicles combined (0.7 to 0.9 Gg year^{-1}; section S8) and includes off-road gasoline/diesel-related contributions (e.g., equipment and generators) in Table 1 and fig. S14. With regard to nontraditional sources, the SOA yields of asphalt-related emissions are considerably higher than estimates for other VCP-related sources on average, whereas VCPs' larger VOC emissions give it a bigger role in potential ozone formation than asphalt-related emissions. In total, VCPs collectively have an estimated SOA production of 7 ± 2.5 Gg year^{-1} in the SoCAB (*2*), which would be appreciably enhanced by the contribution of SOA from asphalt-related emissions (Table 1). Yet, these other key sources of SOA precursors will generally be evenly distributed throughout the year. However, in the SoCAB and other urban climates, these temperature- and radiation-dependent in-use emissions from asphalt will be enhanced during the hottest, sunniest summer periods with the highest photochemical activity and SOA production, giving asphalt-related sources an outsize impact during critical summertime air pollution episodes.

As a result of regulatory policies and technological advances, the evolving portfolio of urban emissions in developed megacities is re-ordering the relative importance of urban SOA precursor sources, especially with increasing attention to nontraditional emissions. Emissions from motor vehicles and other combustion-related sources are only going to decrease further with the phasing out of the oldest, highest emitting vehicles and their replacement with zero emission vehicles, DPF- and DOC-equipped diesel vehicles, and electric vehicles. Furthermore, greater attention to emissions from consumer and commercial products (e.g., VCPs) will further assist in reducing their emissions. Yet, the current consumption of asphalt materials and their emissions are likely to remain the same or increase with infrastructure growth and urban temperature increases driven by climate change and urban heat island effects, thus enhancing their relative impact on urban air quality over time.

MATERIALS AND METHODS

Experimental setup

A temperature-controlled quartz tube furnace (Across International STF1200) was used in short–time scale experiments to investigate the sensitivity of VOC-I/SVOC emissions to temperature. Large chunks of fresh real-world PG 64-22 asphalt, commonly used in U.S. road paving, were obtained during road paving in New Haven, CT (on-site before surface application) and stored in a sealed glass container. During each test, a 12-g asphalt sample measuring 10 cm by 1 cm by 1 cm was weighed using a Mettler Toledo AG285 microscale and inserted into the furnace. The sample weight was determined on the basis of trials to optimize the MS response of all emitted gas-phase chemical constituents. Samples were heated to temperatures ranging from 40° to 200°C to study temperature dependence of asphalt-related emissions across storage, application, and in-use conditions. Preliminary tests with a thermocouple embedded inside the asphalt sample confirmed temperature relationships between the furnace temperature and that of the asphalt sample. A laminar flow of 1 liters per minute (LPM) of zero air (AADCO) was maintained through the tube using an upstream mass flow controller (Alicat) to achieve environmentally relevant emission velocities from the asphalt surface (see section S4 for calculations). In experiments that involved artificial solar irradiation, a 75-W artificial solar spectrum lamp (OTO E27 Sun Lamp) including UVA and UVB radiation was placed above the quartz tube over the sample (section S5 and fig. S15). The solar irradiation on each material's surface during experiments was calculated to be approximately 50 to 60% of that at the Earth's surface on mid-latitudes (section S5). Each gas-phase sample for offline analysis was collected at a flow rate of 125 mL min^{-1} for 10 min at the downstream end of the tube furnace using our custom-made adsorbent tubes described by Sheu *et al.* (*68*). Long–time scale experiments (3 to 7 days) were carried out in a similar custom-made emissions chamber, the construction of which is discussed in section S6 (fig. S16). A summary of measures taken to closely simulate environmental conditions can be found in sections S2 and S3.

Analytical techniques

Custom-packed adsorbent tubes were desorbed using a Gerstel 3.5+ TD system at 300°C using helium as the carrier gas. The analytes were then cryo-focused on a glass wool inlet liner maintained at −100°C using liquid nitrogen, which was then ramped at 400°C min^{-1} to 325°C to inject analytes onto the GC column (DB-5 MS UI, 30 m by 0.32 mm by 0.25 μm). The column was held at 35°C for 5 min before ramping at 10°C min^{-1} to 325°C and held at this maximum temperature for 3 min. The column effluent was directed either into a traditional vacuum pressure EI-MS with unit mass resolution or an APCI-TOF MS operating in positive mode with 25,000 to 40,000 mass resolution (m/Δm) and 2 ppm (parts per million) mass accuracy. The transmission efficiency of I/SVOCs and LVOCs through our analytical system was previously confirmed via extensive trials using Macondo crude oil standard [National Institute of Standards and Technology (NIST) 2779] (*47*). Further details on our integrated sampling-to-analysis system can be found in previous publications (*47*, *68*).

Calibrations

Authentic gas- and liquid-phase standards were used for all calibrations (Apel-Riemer, AccuStandard, and Sigma-Aldrich). For hydrocarbon (C_xH_y) complex mixture speciation, five-point mass calibrations were performed across carbon numbers (C_{10}-C_{32}) and double bond equivalencies (DBEs; 0 to 15) using NIST 2779 Macondo crude oil in the GC-APCI-TOF system (section S9) (*47*). The verified NIST 2779 Macondo crude oil hydrocarbon mass distribution over carbon numbers and DBEs was obtained from literature (*47*, *69*). In addition, C_8-C_{32} *n*-alkanes, naphthalene, 1,5-dimethylnaphthalene, anthracene, pyrene, and fluoranthene standards were run for calibration on GC-EI-MS to quantify known hazardous compounds.

The mass response factors for sulfur- and oxygen-containing complex hydrocarbon mixtures were developed using select individual sulfur- and oxygen-containing hydrocarbon standards and comparing their APCI mass response factors to analogous hydrocarbon compound formulas (see the Supplementary Materials for further details). These included NIST Macondo crude oil (for thiophenes collectively) (*69*) and individual analytical standards of

3-octylthiophene, 4,6-dimethyldibenzothiophene, tetradecane-1-thiol, dodecane-1-thiol, and octadecane-1-thiol. For sulfur-containing hydrocarbon compounds, our mass response factors were consistent with those measured for thiophenes in NIST 2779 Macondo crude oil measured by Worton *et al.* (*69*). Furthermore, given limited information about the exact chemical composition of the oxygen-containing hydrocarbon mixtures, we were unable to assign specific response factors. However, in individual standard comparisons between oxygen-containing and pure hydrocarbon compounds, we found the response factors to be similar, suggesting relatively similar ionization efficiencies for oxygen-containing hydrocarbons compared to pure hydrocarbon aromatic compounds. We also accounted for the transmission efficiencies of functionalized and nonfunctionalized organics through our analytical system, which has been previously established (*47*). Non-aromatic hydrocarbon compounds are more prone to fragmentation and potentially differ in ionization efficiency. In all, we acknowledge that there is uncertainty in calibrations for complex mixtures of oxygen- and sulfur-containing hydrocarbon compounds, which make up only 5 to 15% of emissions at temperatures relevant to life cycles of asphalt materials considered in this study. Thus, the overall emission factors and potential SOA estimates are prone to some additional uncertainty beyond that for the pure hydrocarbon compounds. This is further discussed in section S10.

SUPPLEMENTARY MATERIALS

Supplementary material for this article is available at http://advances.sciencemag.org/cgi/content/full/6/36/eabb9785/DC1

REFERENCES AND NOTES

1. P. Khare, D. R. Gentner, Considering the future of anthropogenic gas-phase organic compound emissions and the increasing influence of non-combustion sources on urban air quality. *Atmos. Chem. Phys.* **18**, 5391–5413 (2018).
2. B. C. Mcdonald, J. A. de Gouw, J. B. Gilman, S. H. Jathar, A. Akherati, C. D. Cappa, J. L. Jimenez, J. Lee-Taylor, P. L. Hayes, S. A. McKeen, Y. Y. Cui, S.-W. Kim, D. R. Gentner, G. Isaacman-VanWertz, A. H. Goldstein, R. A. Harley, G. J. Frost, J. M. Roberts, T. B. Ryerson, M. Trainer, Volatile chemical products emerging as largest petrochemical source of urban organic emissions. *Science* **359**, 760–764 (2018).
3. J. L. Jimenez, M. R. Canagaratna, N. M. Donahue, A. S. H. Prevot, Q. Zhang, J. H. Kroll, P. F. De Carlo, J. D. Allan, H. Coe, N. L. Ng, A. C. Aiken, K. S. Docherty, I. M. Ulbrich, A. P. Grieshop, A. L. Robinson, J. Duplissy, J. D. Smith, K. R. Wilson, V. A. Lanz, C. Hueglin, Y. L. Sun, J. Tian, A. Laaksonen, T. Raatikainen, J. Rautiainen, P. Vaattovaara, M. Ehn, M. Kulmala, J. M. Tomlinson, D. R. Collins, M. J. Cubison, E. J. Dunlea, J. A. Huffman, T. B. Onasch, M. R. Alfarra, P. I. Williams, K. Bower, Y. Kondo, J. Schneider, F. Drewnick, S. Borrmann, S. Weimer, K. Demerjian, D. Salcedo, L. Cottrell, R. Griffin, A. Takami, T. Miyoshi, S. Hatakeyama, A. Shimono, J. Y. Sun, Y. M. Zhang, K. Dzepina, J. R. Kimmel, D. Sueper, J. T. Jayne, S. C. Herndon, A. M. Trimborn, L. R. Williams, E. C. Wood, A. M. Middlebrook, C. E. Kolb, U. Baltensperger, D. R. Worsnop, Evolution of organic aerosols in the atmosphere. *Science* **326**, 1525–1529 (2009).
4. P. K. Ma, Y. Zhao, A. L. Robinson, D. R. Worton, A. H. Goldstein, A. M. Ortega, J. L. Jimenez, P. Zotter, A. S. H. Prévôt, S. Szidat, P. L. Hayes, Evaluating the impact of new observational constraints on P-S/IVOC emissions, multi-generation oxidation, and chamber wall losses on SOA modeling for Los Angeles, CA. *Atmos. Chem. Phys.* **17**, 9237–9259 (2017).
5. Y. Zhao, C. J. Hennigan, A. A. May, D. S. Tkacik, J. A. de Gouw, J. B. Gilman, W. C. Kuster, A. Borbon, A. L. Robinson, Intermediate-volatility organic compounds: A large source of secondary organic aerosol. *Environ. Sci. Technol.* **48**, 13743–13750 (2014).
6. H. Akbari, L. S. Rose, H. Taha, Analyzing the land cover of an urban environment using high-resolution orthophotos. *Landsc. Urban Plan.* **63**, 1–14 (2003).
7. The Freedonia Group, *Asphalt: United States* (The Freedonia Group, Inc., 2015).
8. The Asphalt Institute & European Bitumen Association, *The Bitumen Industry: A Global Perspective: Production, Chemistry, Use, Specification and Occupational Exposure* (Asphalt Institute, 2015).
9. P. T. Nilsson, U. Bergendorf, H. Tinnerberg, E. Nordin, M. Gustavsson, B. Strandberg, M. Albin, A. Gudmundsson, Emissions into the air from bitumen and rubber bitumen—Implications for asphalt workers' exposure. *Ann. Work Expo. Heal.* **62**, 828–839 (2018).
10. R. Rühl, U. Musanke, K. Kolmsee, R. Prieß, D. Breuer, Bitumen emissions on workplaces in Germany. *J. Occup. Environ. Hyg.* **4**, 77–86 (2007).
11. Y. Xu, M. Kåredal, J. Nielsen, M. Adlercreutz, U. Bergendorf, B. Strandberg, A.-B. Antonsson, H. Tinnerberg, M. Albin, Exposure, respiratory symptoms, lung function and inflammation response of road-paving asphalt workers. *Occup. Env. Med.* **75**, 494–500 (2018).
12. K. Elihn, B. Ulvestad, S. Hetland, A. Wallen, B. G. Randem, Exposure to ultrafine particles in asphalt work. *J. Occup. Environ. Hyg.* **5**, 771–779 (2008).
13. A. J. Kriech, J. T. Kurek, H. L. Wissel, L. V. Osborn, G. R. Blackburn, Evaluation of worker exposure to asphalt paving fumes using traditional and nontraditional techniques. *AIHA J.* **63**, 628–635 (2002).
14. J. M. Cavallari, L. M. Zwack, C. R. Lange, R. F. Herrick, M. D. Mcclean, Temperature-dependent emission concentrations of polycyclic aromatic hydrocarbons in paving and built-up roofing asphalts. *Ann. Occup. Hyg.* **56**, 148–160 (2012).
15. J. M. Cavallari, L. V. Osborn, J. E. Snawder, A. J. Kriech, L. D. Olsen, R. F. Herrick, M. D. McClean, Predictors of airborne exposures to polycyclic aromatic compounds and total organic matter among hot-mix asphalt paving workers and influence of work conditions and practices. *Ann. Occup. Hyg.* **56**, 138–147 (2012).
16. D. Trumbore, A. Jankousky, E. L. Hockman Jr., R. Sanders, J. Calkin, S. Szczepanik, R. Owens, Emission factors for asphalt-related emissions in roofing manufacturing. *Environ. Prog.* **24**, 268–278 (2005).
17. National Asphalt Pavement Association, *Greenhouse Gas Calculator*; http://www.asphaltpavement.org/GHGC.
18. S. Kishan, A. Burnette, S. Fincher, M. Sabisch, W. Crews, R. Snow, M. Zmud, R. Santos, S. Bricka, E. Fujita, D. Campbell, P. Arnott, "Kansas City PM characterization study final report" (Report No. EPA420-R-08e009, U.S. EPA, 2008).
19. A. L. Jankousky, *Proposed Emission Factors for Criteria Pollutants and Hazardous Air Pollutants from Asphalt Roofing Manufacturing* (The Asphalt Roofing Manufacturers Association, 2003).
20. C. Lange, M. Stroup-Gardiner, L. Cr, Quantification of potentially odorous volatile organic compounds from asphalt binders using head-space gas chromatography. *J. Test. Eval.* **33**, 101–109 (2005).
21. C. R. Lange, M. Stroup-Gardiner, Temperature-dependent chemical-specific emission rates of aromatics and polyaromatic hydrocarbons (PAHs) in bitumen fume. *J. Occup. Environ. Hyg.* **4**, 72–76 (2007).
22. A. Preiss, W. Koch, H. Kock, M. Elend, M. Raabe, G. Pohlmann, Collection, validation and generation of bitumen fumes for inhalation studies in rats part 1: Workplace samples and validation criteria. *Ann. Occup. Hyg.* **50**, 789–804 (2006).
23. E. Gasthauer, M. Mazé, J. P. Marchand, J. Amouroux, Characterization of asphalt fume composition by GC/MS and effect of temperature. *Fuel* **87**, 1428–1434 (2008).
24. J. Kurek, A. Kriech, H. Wissel, L. Osborn, G. Blackburn, Laboratory generation and evaluation of paving asphalt fumes. *Transp. Res. Rec. J. Transp. Res. Board* **1661**, 35–40 (1999).
25. A. M. Kitto, M. Pirbazari, B. N. Badriyha, V. Ravindran, R. Tyner, C. E. Synolakis, Emissions of volatile and semi-volatile organic compounds and particulate matter from hot asphalts. *Environ. Technol.* **18**, 121–138 (1997).
26. European Bitumen Association, *Life Cycle Inventory: Bitumen* (The European Bitumen Association, 2012).
27. X. He, D. Hochstein, Q. Ge, A. W. Ali, F. Chen, H. Yin, Accelerated aging of asphalt by UV photo-oxidation considering moisture and condensation effects. *J. Mater. Civ. Eng.* **30**, 04017261 (2018).
28. J.-F. Masson, J. R. Woods, P. Collins, I. L. Al-Qadi, Accelerated aging of bituminous sealants: Small kettle aging. *Int. J. Pavement Eng.* **9**, 365–371 (2008).
29. B. Peng, C. Cai, G. Yin, W. Li, Y. Zhan, Evaluation system for CO_2 emission of hot asphalt mixture. *J. Traffic Transp. Eng.* **2**, 116–124 (2015).
30. M. R. Mohd Hasan, Z. You, Estimation of cumulative energy demand and green house gas emissions of ethanol foamed WMA using life cycle assessment analysis. *Construct. Build Mater.* **93**, 1117–1124 (2015).
31. S. C. Tyler, D. C. Lowe, E. Dlugokencky, P. R. Zimmerman, R. J. Cicerone, Methane and carbon monoxide emissions from asphalt pavement: Measurements and estimates of their importance to global budgets. *J. Geophys. Res.* **95**, 14007–14014 (1990).
32. B. Yu, S. Wang, X. Gu, Estimation and uncertainty analysis of energy consumption and CO_2 emission of asphalt pavement maintenance. *J. Clean. Prod.* **189**, 326–333 (2018).
33. W. Zeng, S. Wu, J. Wen, Z. Chen, The temperature effects in aging index of asphalt during UV aging process. *Construct. Build Mater.* **93**, 1125–1131 (2015).
34. J. Hu, S. Wu, Q. Liu, M. I. G. Hernández, W. Zeng, S. Nie, J. Wan, D. Zhang, Y. Li, The effect of ultraviolet radiation on bitumen aging depth. *Materials* **11**, 747 (2018).
35. The Freedonia Group, *Asphalt: US Industry Study with Forecasts for 2019 & 2024. Study #3304* (The Freedonia Group, Inc., 2015).
36. The Freedonia Group, *World Asphalt (Bitumen): Industry Study with Forecasts for 2019 and 2024. Study#3351* (The Freedonia Group, Inc., 2015).
37. M. Pomerantz, B. Pon, H. Akbari, S.-C. Chang, *The Effect of Pavements' Temperatures on Air Temperatures in Large Cities* (Lawrence Berkeley National Laboratory, 2000).

38. H. Higashiyama, M. Sano, F. Nakanishi, O. Takahashi, S. Tsukuma, Field measurements of road surface temperature of several asphalt pavements with temperature rise reducing function. *Case Stud. Constr. Mater.* **4**, 73–80 (2016).
39. J. J. Berens, Thermal contact burns from streets and highways. *JAMA* **214**, 2025–2027 (1970).
40. J. Vega Jr., P. Chestovich, S. Saquib, D. Fraser, A 5-year review of pavement burns from a desert burn center. *J. Burn Care Res.* **40**, 422–426 (2019).
41. E. Toraldo, E. Mariani, S. Alberti, M. Crispino, Experimental investigation into the thermal behavior of wearing courses for road pavements due to environmental conditions. *Construct. Build Mater.* **98**, 846–852 (2015).
42. D. Parker, J. Sonne, J. Sherwin, *Demonstration of Cooling Savings of Light Colored Roof Surfacing in Florida Commercial Buildings: Retail Strip Mall* (Florida Solar Energy Center/ University of Central Florida, 1997); http://www.fsec.ucf.edu/en/publications/pdf/ FSEC-CR-964-97.pdf.
43. S. R. Gaffin, M. Imhoff, C. Rosenzweig, R. Khanbilvardi, A. Pasqualini, A. Y. Y. Kong, D. Grillo, A. Freed, D. Hillel, E. Hartung, Bright is the new black—Multi-year performance of high-albedo roofs in an urban climate. *Environ. Res. Lett.* **7**, 014029 (2012).
44. D. R. Gentner, G. Isaacman, D. R. Worton, A. W. H. Chan, T. R. Dallmann, L. Davis, S. Liu, D. A. Day, L. M. Russell, K. R. Wilson, R. Weber, A. Guha, R. A. Harley, A. H. Goldstein, Elucidating secondary organic aerosol from diesel and gasoline vehicles through detailed characterization of organic carbon emissions. *Proc. Natl. Acad. Sci. U.S.A.* **109**, 18318–18323 (2012).
45. J. A. Wess, L. D. Olsen, D. Marie, H. Sweeney, *ASPHALT (BITUMEN)* (World Health Organization, 2004).
46. A. J. Kriech, C. A. Schreiner, L. V. Osborn, A. J. Riley, Assessing cancer hazards of bitumen emissions—A case study for complex petroleum substances. *Crit. Rev. Toxicol.* **48**, 121–142 (2017).
47. P. Khare, A. Marcotte, R. Sheu, A. N. Walsh, J. C. Ditto, D. R. Gen, Advances in offline approaches for trace measurements of complex organic compound mixtures via soft ionization and high-resolution tandem mass spectrometry. *J. Chromatogr. A* **1598**, 163–174 (2019).
48. Boundary layer (atmospheric) and air pollution| urban heat islands, in *Encyclopedia of Atmospheric Sciences* (Elsevier, 2015).
49. D. Helmig, B. Balsley, K. Davis, L. R. Kuck, M. Jensen, J. Bognar, T. Smith Jr., R. V. Arrieta, R. Rodríguez, J. W. Birks, Vertical profiling and determination of landscape fluxes of biogenic nonmethane hydrocarbons within the planetary boundary layer in the Peruvian Amazon. *J. Geophys. Res. Atmos.* **103**, 25519–25532 (1998).
50. T. K. Kuhn, E. S. Krull, A. Bowater, K. Grice, G. Gleixner, The occurrence of short chain *n*-alkanes with an even over odd predominance in higher plants and soils. *Org. Geochem.* **41**, 88–95 (2010).
51. Y. Zhao, F. Wei, Y. Yu, Effects of reaction time and temperature on carbonization in asphaltene pyrolysis. *J. Petrol. Sci. Eng.* **74**, 20–25 (2010).
52. A. Boytsova, N. Kondrasheva, J. Ancheyta, Pyrolysis kinetics of heavy oil asphaltenes under steam atmosphere at different pressures. *Energy Fuels* **32**, 1132–1138 (2018).
53. M. Schmitt, P. R. Erickson, K. McNeill, Triplet-state dissolved organic matter quantum yields and lifetimes from direct observation of aromatic amine oxidation. *Environ. Sci. Technol.* **51**, 13151–13160 (2017).
54. E. Appiani, K. McNeill, Photochemical production of singlet oxygen from particulate organic matter. *Environ. Sci. Technol.* **49**, 3514–3522 (2015).
55. R. Kaur, J. R. Labins, S. S. Helbock, W. Jiang, K. J. Bein, Q. Zhang, C. Anastasio, Photooxidants from brown carbon and other chromophores in illuminated particle extracts. *Atmos. Chem. Phys.* **19**, 6579–6594 (2019).
56. D. E. Nicodem, C. L. B. Guedes, M. Conceição, Z. Fernandes, D. Severino, R. J. Correa, M. C. Coutinho, J. Silva, Photochemistry of petroleum. *Prog. React. Kinet. Mech.* **26**, 219–238 (2001).
57. A. Laskin, J. Laskin, S. A. Nizkorodov, Chemistry of atmospheric brown carbon. *Chem. Rev.* **115**, 4335–4382 (2015).
58. T. Atsumi, I. Iwakura, S. Fujisawa, T. Ueha, The production of reactive oxygen species by irradiated camphorquinone-related photosensitizers and their effect on cytotoxicity. *Arch. Oral Biol.* **46**, 391–401 (2001).
59. S. Garg, A. L. Rose, T. D. Waite, Production of reactive oxygen species on photolysis of dilute aqueous quinone solutions. *Photochem. Photobiol.* **83**, 904–913 (2007).
60. J. Sasaki, S. M. Aschmann, E. S. C. Kwok, R. Atkinson, J. Arey, Products of the gas-phase OH and NO_3 radical-initiated reactions of naphthalene. *Environ. Sci. Technol.* **31**, 3173–3179 (1997).
61. K. E. Kautzman, J. D. Surratt, M. N. Chan, A. W. H. Chan, S. P. Hersey, P. S. Chhabra, N. F. Dalleska, P. O. Wennberg, R. C. Flagan, J. H. Seinfeld, Chemical composition of gas- and aerosol-phase products from the photooxidation of naphthalene. *J. Phys. Chem. A* **114**, 913–934 (2010).
62. R. P. Schwarzenbach, P. M. Gschwend, D. M. Imboden, Direct photolysis in aquatic systems, in *Environmental Organic Chemistry* (Wiley, 2016), pp. 773–813.
63. What is PG System?, California Department of Transportation; http://www.dot.ca.gov/hq/ oppd/pavement/pgb.htm.
64. Y. Zhao, N. T. Nguyen, A. A. Presto, C. J. Hennigan, A. A. May, A. L. Robinson, Intermediate volatility organic compound emissions from on-road gasoline vehicles and small off-road gasoline engines. *Environ. Sci. Technol.* **50**, 4554–4563 (2016).
65. D. R. Gentner, D. R. Worton, G. Isaacman, L. C. Davis, T. R. Dallmann, E. C. Wood, S. C. Herndon, A. H. Goldstein, R. A. Harley, Chemical composition of gas-phase organic carbon emissions from motor vehicles and implications for ozone production. *Environ. Sci. Technol.* **47**, 11837–11848 (2013).
66. D. R. Gentner, S. H. Jathar, T. D. Gordon, R. Bahreini, D. A. Day, I. E. Haddad, P. L. Hayes, S. M. Pieber, S. M. Platt, J. de Gouw, A. H. Goldstein, R. A. Harley, J. L. Jimenez, A. S. H. Prévôt, A. L. Robinson, Review of urban secondary organic aerosol formation from gasoline and diesel motor vehicle emissions. *Environ. Sci. Technol.* **51**, 1074–1093 (2017).
67. P. L. Hayes, A. G. Carlton, K. R. Baker, R. Ahmadov, R. A. Washenfelder, S. Alvarez, B. Rappenglück, J. B. Gilman, W. C. Kuster, J. A. de Gouw, P. Zotter, A. S. H. Prévôt, S. Szidat, T. E. Kleindienst, J. H. Offenberg, P. K. Ma, J. L. Jimenez, Modeling the formation and aging of secondary organic aerosols in Los Angeles during CalNex 2010. *Atmos. Chem. Phys.* **15**, 5773–5801 (2015).
68. R. Sheu, A. Marcotte, P. Khare, S. Charan, J. C. Ditto, D. R. Gentner, Advances in offline approaches for speciated measurements of trace gas-phase organic compounds via an integrated sampling-to-analysis system. *J. Chromatogr. A* **1575**, 80–90 (2018).
69. D. R. Worton, H. Zhang, G. I.-V. Wertz, A. W. H. Chan, K. R. Wilson, A. H. Goldstein, Comprehensive chemical characterization of hydrocarbons in NIST standard reference material 2779 gulf of mexico crude oil. *Environ. Sci. Technol.* **49**, 13130–13138 (2015).
70. California Air Resources Board, Mobile Source Emission Inventory—EMFAC2017 Web Database; https://arb.ca.gov/emfac/2017/ [accessed 6 June 2020].
71. California Air Resources Board, OFFROAD2017-ORION Web Database; https://www.arb.ca.gov/orion/?_ga=2.255852811.1420576813.1591370242-1958507417.1591370188 [accessed 6 June 2020].
72. California Air Resources Board, Almanac Emission Projection Data; https://www.arb.ca.gov/app/emsinv/2017/emssumcat_query.php?F_YR=2020&F_DIV=-4&F_SEASON=A&SP=SIP105ADJ&F_AREA=AB&F_AB=SC#3 [accessed 7 June 2020].
73. Transportation Research Board of the National Academies, *Practical Approaches to Hot-Mix Asphalt Mix Design and Production Quality Control Testing* (Transportation Research Board of the National Academies, 2007).
74. Transportation Research Board of the National Academies, *SUPERPAVE: Performance by Design* (Transportation Research Board of the National Academies, 2005).
75. U.S. Environmental Protection Agency, *Reducing Urban Heat Islands: Compendium of Strategies-Cool Pavements* (U.S. Environmental Protection Agency, 2008).
76. Y.-J. Kim, B.-J. Kim, Y.-S. Shin, H.-W. Kim, G.-T. Kim, S.-J. Kim, A case study of environmental characteristics on urban road-surface and air temperatures during heat-wave days in Seoul. *Atmos. Ocean. Sci. Lett.* **12**, 261–269 (2019).
77. R. Watkins, J. Palmer, M. Kolokotroni, Increased temperature and intensification of the urban heat island: Implications for human comfort and urban design. *Built Environ.* **33**, 85–96 (2007).
78. U.S. EPA, Heat island impacts, heat island effect; https://www.epa.gov/heat-islands/ heat-island-impacts [accessed 12 February 2020].
79. W. B. Rose, *Measured Summer Values of Sheathing and Shingle Temperatures for Residential Attics and Cathedral Ceilings, Buildings VIII/Low-Slope Roofs-Principles* (Buildings VIII Conference 2001 organized by the Oak Ridge National Laboratory).
80. F. Lehner, C. Deser, B. M. Sanderson, Future risk of record-breaking summer temperatures and its mitigation. *Clim. Change* **146**, 363–375 (2018).
81. M. R. Haylock, N. Hofstra, A. M. G. K. Tank, E. J. Klok, P. D. Jones, M. New, A European daily high-resolution gridded data set of surface temperature and precipitation for 1950–2006. *J. Geophys. Res.* **113**, D20119 (2008).
82. R. Sheu, A. Marcotte, P. Khare, S. Charan, J. C. Ditto, D. R. Gentner, Advances in offline approaches for chemically speciated measurements of trace gas-phase organic compounds via adsorbent tubes in an integrated sampling-to-analysis system. *J. Chromatogr. A* **1575**, 80–90 (2018).
83. C. J. Weschler, W. W. Nazaroff, Semivolatile organic compounds in indoor environments. *Atmos. Environ.* **42**, 9018–9040 (2008).
84. D. E. Freed, L. Burcaw, Y.-Q. Song, Scaling laws for diffusion coefficients in mixtures of alkanes. *Phys. Rev. Lett.* **94**, 067602 (2005).
85. T. G. Hiss, E. L. Cussler, Diffusion in high viscosity liquids. *AIChE J.* **19**, 698–703 (1973).
86. M. Iwahashi, Y. Yamaguchi, Y. Ogura, M. Suzuki, Dynamical structures of normal alkanes, alcohols, and fatty acids in the liquid state as determined by viscosity, self-diffusion coefficient, infrared spectra, and ^{13}CNMR spin-lattice relaxation time measurements. *Bull. Chem. Soc. Jpn.* **63**, 2154–2158 (1990).
87. K. Falk, B. Coasne, R. Pellenq, F.-J. Ulm, L. Bocquet, Subcontinuum mass transport of condensed hydrocarbons in nanoporous media. *Nat. Commun.* **6**, 6949 (2015).

88. M. A. Elseifi, I. L. Al-Qadi, S.-H. Yang, S. H. Carpenter, Validity of asphalt binder film thickness concept in hot-mix asphalt. *Transp. Res. Rec. J. Transp. Res. Board* **2057**, 37–45 (2008).
89. P. G. Nicholson, Admixture soil improvement, in *Soil Improvement and Ground Modification Methods* (Elsevier, 2015), pp. 231–288.
90. D. R. Gentner, R. A. Harley, A. M. Miller, A. H. Goldstein, Diurnal and seasonal variability of gasoline-related volatile organic compound emissions in riverside, California. *Environ. Sci. Technol.* **43**, 4247–4252 (2009).
91. Y. Zhao, R. Saleh, G. Saliba, A. A. Presto, T. D. Gordon, G. T. Drozd, A. H. Goldstein, N. M. Donahue, A. L. Robinson, Reducing secondary organic aerosol formation from gasoline vehicle exhaust. *Proc. Natl. Acad. Sci. U.S.A.* **114**, 6984–6989 (2017).
92. J. H. Kroll, J. H. Seinfeld, Chemistry of secondary organic aerosol: Formation and evolution of low-volatility organics in the atmosphere. *Atmos. Environ.* **42**, 3593–3624 (2008).
93. U.S. Environmental Protection Agency, *EPI Suite™-Estimation Program Interface, Predictive Models and Tools for Assessing Chemicals under the Toxic Substances Control Act (TSCA)* (2020).

Acknowledgments: We thank the Yale Office of Facilities for helping acquire the PG 64-22 road asphalt from a road-paving event in New Haven, CT; the CACES Center (Carnegie Mellon University) and their team for helping acquire road asphalt samples from Pittsburgh, PA; and J. Kim (Yale), G. Ban-Weiss (USC), and A. Chan (University of Toronto) for their helpful discussions. **Funding:** We thank the Yale SEARCH Center, U.S. EPA, and NSF (AWD0001666) for support, as well as GERSTEL for collaboration and support with the TD 3.5+. This publication was developed under Assistance Agreements RD835871 (Yale University) and 83587301 (Carnegie Mellon University) awarded by the U.S. Environmental Protection Agency. It has not been formally reviewed by EPA. The views expressed in this document are solely those of the authors and do not necessarily reflect those of the Agency. EPA does not endorse any products or commercial services mentioned in this publication. **Author contributions:** P.K. and D.R.G. conceived the study and designed laboratory experiments and the experimental setup. P.K., J.M., A.A.P., and D.R.G. acquired the asphalt materials. P.K. and R.S. (New Haven, CT) and J.M. and A.A.P. (Pittsburgh, PA) conducted on-site gas-phase sampling. P.K. collected gas-phase samples in the laboratory. Subsequently, P.K., J.M., and M.H. conducted the analysis of data acquired using EI-MS and APCI-TOF. P.K. and D.R.G. interpreted the data and wrote the paper. All authors commented on and discussed the manuscript to help refine the interpretation and presentation of results. **Competing interests:** The authors declare that they have no competing interests. **Data and materials availability:** All data needed to evaluate the conclusions in the paper are present in the paper and/or the Supplementary Material, including speciated emission profiles. Additional data related to this paper can be provided by the authors upon request.

Submitted 1 April 2020
Accepted 21 July 2020
Published 2 September 2020
10.1126/sciadv.abb9785

Citation: P. Khare, J. Machesky, R. Soto, M. He, A. A. Presto, D. R. Gentner, Asphalt-related emissions are a major missing nontraditional source of secondary organic aerosol precursors. *Sci. Adv.* **6**, eabb9785 (2020).

Science Advances

Asphalt-related emissions are a major missing nontraditional source of secondary organic aerosol precursors

Peeyush Khare, Jo Machesky, Ricardo Soto, Megan He, Albert A. Presto and Drew R. Gentner

Sci Adv **6** (36), eabb9785.
DOI: 10.1126/sciadv.abb9785

Science Advances (ISSN 2375-2548) is published by the American Association for the Advancement of Science, 1200 New York Avenue NW, Washington, DC 20005. The title *Science Advances* is a registered trademark of AAAS.